Shape mixing and β-decay properties of neutron-deficient Kr and Sr isotopes

P. Sarriguren

Instituto de Estructura de la Materia, CSIC, Serrano 123, E-28006 Madrid, Spain

Gamow-Teller strength distributions and β-decay half-lives in neutron-deficient Kr and Sr isotopes are investigated within a deformed quasiparticle random phase approximation. The approach is based on a self-consistent Skyrme Hartree-Fock mean field with pairing correlations and residual separable particle-hole and particle-particle forces. A simple two-level model is used to mix the nuclear shapes into the physical ground state. Good agreement with experiment is found with shape mixing coefficients which are consistent with those obtained phenomenologically from mixing of rotational bands.

PACS number(s): 21.60.Jz, 23.40.Hc, 27.50.+e

I. INTRODUCTION

Neutron-deficient isotopes in the $A = 70$–80 mass region are known to be interesting examples where the equilibrium shape of the nucleus is the result of a critical interplay between various nuclear structure effects [1]. The evolution of the nuclear shape in isotopic chains is rather involved due to the existence of shell gaps at nucleon numbers 34, 36, 38, and 40. Thus, adding or removing a few nucleons may lead to shape transitions in neighboring nuclei. Shape coexistence is also present in this mass region, where competing prolate, oblate, and spherical shapes are expected in the same nucleus at close energies. Calculations of the equilibrium configurations in this mass region have been performed within different approaches, such as the configuration-dependent shell-correction approach with deformed Woods-Saxon potentials [2], self-consistent deformed Skyrme mean-field calculations [3,4], Hartree-Fock-Bogoliubov calculations with the Gogny force [5], relativistic mean-field calculations [6], or the self-consistent complex excited VAMPIR approach [7].

The first experimental evidence of shape coexistence in neutron-deficient Kr isotopes was reported in Ref. [8] from irregularities observed at the bottom of the rotational bands. Since then, a great deal of data on the low-lying excitation spectrum, including transition probabilities, have become available [9–12]. One of the experimental indications revealing the existence of shape coexistence in even-even nuclei is the observation of low-lying 0^+ excited states. Each of the 0^+ states is interpreted as a ground state corresponding to a different shape. Experimental evidences for 0^+ shape isomers in Kr isotopes have been reported in Refs. [9–11]. These states are connected by electric monopole ($E0$) transitions, whose strength is related to the change in the rms radius of the nucleus between initial and final states and carries information about the change in deformation and the overlap of the wave functions. The relationship between $E0$ strength and shape mixing has been investigated in Refs. [13–15]. In these references, shape mixing and shape coexistence were analyzed in terms of a two-level model, which was shown to be a simple but successful method to interpret the phenomenology. In this model, the strength is related to the amount of mixing of configurations with different deformations in the physical states. This simple two-level mixing model has been also

successfully applied to understand the low-energy spectra of neutron-deficient Kr isotopes [12]. In these isotopes, regular bands are observed at high spins, which is a characteristic of well deformed shapes, but for the lowest states the regularity is lost, which is interpreted as evidence for a perturbation from other close states. The anomaly at low spin observed in the systematics of the moments of inertia (see Fig. 3.37 in Ref. [15]) has also been interpreted as an evidence for mixed ground states in the lightest Sr isotopes. This mixing predicts that $E0$ transition strengths should be observable in neutron-deficient Sr isotopes. An experiment similar to the study of the ^{74}Rb decay to ^{74}Kr [16] would be very helpful for the ^{78}Y decay to ^{78}Sr.

The decay properties of nuclei in this mass region have been also investigated both theoretically [17–20] and experimentally [21–24]. Deformation has been identified in those works as a relevant issue to understand β-decay properties. In particular, the nuclear deformation is crucial to perform reliable calculations of nuclear reaction rates and β-decay half-lives in nuclei involved in the rapid-proton capture (rp) process of relevance in X-ray burst scenarios [25,26].

In this work we investigate the decay properties of neutron-deficient Kr (^{72,74}Kr) and Sr (^{76,78}Sr) isotopes within a deformed Hartree-Fock (HF) with Skyrme interactions and pairing correlations in BCS approximation. Residual spin-isospin interactions are also included and treated in quasiparticle random phase approximation (QRPA) [18,27–29]. In Sec. II a brief review of the theoretical formalism is presented. Section III contains the results obtained within this approach for the potential energy curves, electric monopole strengths, Gamow-Teller (GT) strength distributions, and β-decay half-lives. The results are discussed in terms of shape mixing using a two-level model. Section IV summarizes the main conclusions.

II. THEORETICAL FORMALISM

In this section we summarize briefly the theory involved in the microscopic calculations. More details can be found in Ref. [18]. The method consists in a self-consistent formalism based on a deformed Hartree-Fock mean field obtained with Skyrme interactions, including pairing correlations in the BCS approximation. The single-particle energies, wave functions,

and occupation probabilities are generated from this mean field. Two Skyrme forces are considered in this paper to quantify the theoretical uncertainties caused by the use of different effective interactions. One is the force Sk3 [30], which is one of the simplest and oldest parametrizations, and has been successfully tested against many nuclear properties in spherical and deformed nuclei. The other force is SLy4 [31], which is an example of one of the most recent parametrizations including selected properties of unstable nuclei in the adjusting procedure.

The solution of the HF equation is found using the formalism developed in Ref. [32], assuming time reversal and axial symmetry. The single-particle wave functions are expanded in terms of the eigenstates of an axially symmetric harmonic oscillator in cylindrical coordinates, using 12 major shells. The method also includes pairing between like nucleons in BCS approximation with fixed gap parameters for protons and neutrons, which are determined phenomenologically from the odd-even mass differences through a symmetric five term formula involving the experimental binding energies [33].

The energy surfaces are analyzed as a function of the quadrupole deformation. For that purpose, constrained HF calculations are performed with a quadratic constraint [34]. The HF energy is minimized under the constraint of keeping fixed the nuclear deformation. Calculations for GT strengths are performed subsequently for the equilibrium shapes of each nucleus, that is, for the solutions, in general deformed, for which minima are obtained in the energy surfaces. Since decays connecting different shapes are disfavored, similar shapes are assumed for the ground state of the parent nucleus and for all populated states in the daughter nucleus.

To describe GT transitions, a spin-isospin residual interaction is added to the mean field. This interaction contains two parts, particle-hole (ph) and particle-particle (pp). The interaction in the ph channel is responsible for the position and structure of the GT resonance [18,28] and it can be derived consistently from the same Skyrme interaction used to generate the mean field, through the second derivatives of the energy density functional with respect to the one-body densities. The ph residual interaction is finally written in a separable form by averaging the Landau-Migdal resulting force over the nuclear volume, as explained in Ref. [18]. The pp part is a neutron-proton pairing force in the $J^\pi = 1^+$ coupling channel, which is also introduced as a separable force [29].

$$V_{GT}^{ph} = 2\chi_{GT}^{ph} \sum_{K=0,\pm 1} (-1)^K \beta_K^+ \beta_{-K}^-,$$
$$\beta_K^+ = \sum_{\pi\nu} \langle\nu|\sigma_K|\pi\rangle a_\nu^+ a_\pi, \quad (1)$$

$$V_{GT}^{pp} = -2\kappa_{GT}^{pp} \sum_K (-1)^K P_K^+ P_{-K},$$
$$P_K^+ = \sum_{\pi\nu} \langle\pi|(\sigma_K)^+|\nu\rangle a_\nu^+ a_{\bar\pi}^+. \quad (2)$$

The coupling strengths used in this work are $\chi_{GT}^{ph} = 0.17$ MeV and $\kappa_{GT}^{pp} = 0.03$ MeV.

The proton-neutron QRPA phonon operator for GT excitations in even-even nuclei is written as

$$\Gamma_{\omega_K}^+ = \sum_{\pi\nu} \left[X_{\pi\nu}^{\omega_K} \alpha_\nu^+ \alpha_{\bar\pi}^+ + Y_{\pi\nu}^{\omega_K} \alpha_{\bar\nu} \alpha_\pi \right], \quad (3)$$

where $\alpha^+(\alpha)$ are quasiparticle creation (annihilation) operators, ω_K are the QRPA excitation energies, and $X_{\pi\nu}^{\omega_K}$, $Y_{\pi\nu}^{\omega_K}$ the forward and backward amplitudes, respectively. For even-even nuclei the allowed GT transition amplitudes in the intrinsic frame connecting the QRPA ground state $|0\rangle [\Gamma_{\omega_K}|0\rangle = 0]$ to one-phonon states $|\omega_K\rangle [\Gamma_{\omega_K}^+|0\rangle = |\omega_K\rangle]$, are given by

$$\langle\omega_K|\sigma_K t^\pm|0\rangle = \mp M_\pm^{\omega_K}, \quad (4)$$

where

$$M_-^{\omega_K} = \sum_{\pi\nu} \left(q_{\pi\nu} X_{\pi\nu}^{\omega_K} + \tilde{q}_{\pi\nu} Y_{\pi\nu}^{\omega_K} \right),$$
$$M_+^{\omega_K} = \sum_{\pi\nu} \left(\tilde{q}_{\pi\nu} X_{\pi\nu}^{\omega_K} + q_{\pi\nu} Y_{\pi\nu}^{\omega_K} \right), \quad (5)$$

with

$$\tilde{q}_{\pi\nu} = u_\nu v_\pi \Sigma_K^{\nu\pi}, \quad q_{\pi\nu} = v_\nu u_\pi \Sigma_K^{\nu\pi}, \quad (6)$$

ν's are occupation amplitudes ($u^2 = 1 - v^2$) and $\Sigma_K^{\nu\pi}$ spin matrix elements connecting neutron and proton states with spin operators

$$\Sigma_K^{\nu\pi} = \langle\nu|\sigma_K|\pi\rangle. \quad (7)$$

The solutions of the QRPA equations are found by solving first a dispersion relation of fourth order in the excitation energies ω. The technical procedure to solve the QRPA equations is described in detail in Ref. [29]. The Ikeda sum rule [35] is always fulfilled in these calculations.

The GT strength $B_\omega(GT^\pm)$ in the laboratory system for a transition $I_i K_i(0^+0) \to I_f K_f(1^+K)$ can be obtained as

$$B_\omega(GT^\pm) = \sum_{\omega_K} [\langle\omega_{K=0}|\sigma_0 t^\pm|0\rangle^2 \delta(\omega_{K=0} - \omega)$$
$$+ 2\langle\omega_{K=1}|\sigma_1 t^\pm|0\rangle^2 \delta(\omega_{K=1} - \omega)], \quad (8)$$

in $[g_A^2/4\pi]$ units. To obtain this expression, the initial and final states in the laboratory frame have been expressed in terms of the intrinsic states using the Bohr-Mottelson factorization [36]. The effect of angular momentum projection is then, to a large extent, taken into account.

The β-decay half-life is obtained by summing up all the allowed transition probabilities weighted with some phase space factors up to states in the daughter nucleus with excitation energies lying below the corresponding Q-energy,

$$T_{1/2}^{-1} = \frac{1}{D} \sum_\omega f(Z, \omega)\{B_\omega(F) + [0.77(g_A/g_V)_{\text{free}}]^2 B_\omega(GT)\}, \quad (9)$$

where $D = 6200$ s and 0.77 is a standard quenching factor that takes into account in an effective way all the correlations [37] which are not properly considered in the present approach. Since Fermi contributions are very small, the bare results can be recovered by scaling the results in this paper for $B(GT)$ and $T_{1/2}$ with the square of this quenching factor.
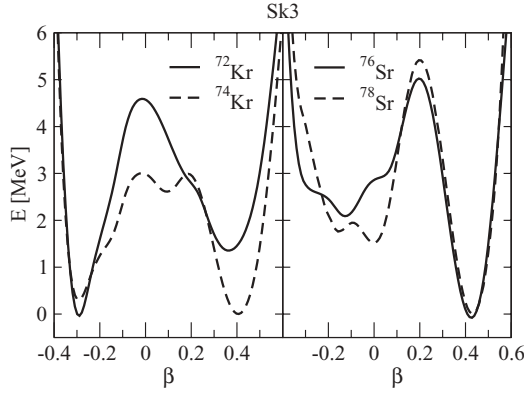
FIG. 1. Potential energy curves for ^{72,74}Kr (left panel) and ^{76,78}Sr (right panel) obtained from constrained HF+BCS calculations with the Skyrme force Sk3. Beta is the quadrupole deformation.

In β^+/EC decay, the Fermi integral $f(Z, \omega)$ consists of two parts, positron emission and electron capture. In this work they are computed numerically for each value of the energy, as explained in Ref. [38]. The inclusion of the Fermi strength $B_\omega(F^+) = [g_V^2/4\pi]\langle\omega|t^+|0\rangle^2$ in the β^+/EC half-lives becomes important only for nuclei with $Z > N$. The calculation of these contributions in our case shows that they are negligible in the $N = Z + 2$ isotopes (^{74}Kr,^{78}Sr) and represents only a few percent correction in the case $N = Z$ (^{72}Kr,^{76}Sr).

III. RESULTS

A. Potential energy curves and electric monopole strength

The potential energy curves corresponding to the force Sk3 (SLy4) for the isotopes ^{72,74}Kr and ^{76,78}Sr can be seen in Fig. 1 (Fig. 2). We obtain an oblate ground state in ^{72}Kr with a prolate local minimum at higher energy. In the case of ^{74}Kr, the oblate and prolate solutions are practically degenerate in the Sk3 case, while SLy4 predicts an oblate shape in the ground state. The Sr isotopes show for Sk3 a prolate ground state and a second oblate (spherical) minimum for ^{76}Sr (^{78}Sr).
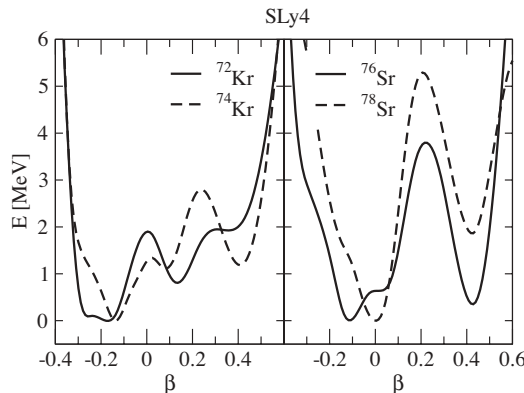

FIG. 2. Same as in Fig. 1 for SLy4.

In the case of SLy4 the oblate and prolate solutions are practically degenerate in ^{76}Sr. The spherical shape becomes the ground state in the case of ^{78}Sr. These results are in qualitative agreement with similar results obtained in this mass region from different methods [2–7,39]. In all of these studies ^{72}Kr is found to be oblate in its ground state with a prolate solution at higher energy. ^{74}Kr is found to exhibit prolate and oblate solutions close in energy. Both ^{76}Sr and ^{78}Sr show prolate deformations in their ground states with oblate and spherical minima at higher energies, respectively. These features are also in agreement with experiment, where similar shape changes have been observed in this region [12,40].

As it was mentioned in the Introduction, the two-level mixing model has been successfully used to interpret the low-lying excitation spectra of neutron-deficient Kr isotopes measured in Coulomb excitation experiments [12]. Coulomb excitation is a suitable method to distinguish between different shapes of the nucleus and to verify the shape coexistence scenario in light Kr isotopes. The analysis carried out in Ref. [12] was based on the assumption of two regular rotational bands with collective intraband transitions and zero matrix elements between the intrinsic states of the different bands. It confirms the prolate-oblate shape coexistence scenario in ^{74}Kr, with an extracted squared mixing amplitude for the prolate configuration $\lambda = 0.48$. The squared amplitude is only $\lambda = 0.10$ (mostly oblate) in ^{72}Kr, as extracted phenomenologically in Ref. [11].

The electric monopole operator can be expressed in terms of single-nucleon degrees of freedom as

$$T(E0) = \sum_k e_k r_k^2. \tag{10}$$

The diagonal matrix elements of this operator give information about nuclear radii. The nondiagonal matrix elements give $E0$ transition amplitudes. If we consider the mixing of two 0^+ intrinsic deformed configurations, the mixed or physical states (ground state and excited state) can be written as a linear combination of them,

$$\begin{aligned} |0^+_{\text{g.s.}}\rangle &= \sqrt{\lambda}|0^+_{\text{prol}}\rangle + \sqrt{1-\lambda}|0^+_{\text{obl}}\rangle, \\ |0^+_{\text{exc}}\rangle &= \sqrt{1-\lambda}|0^+_{\text{prol}}\rangle - \sqrt{\lambda}|0^+_{\text{obl}}\rangle, \end{aligned} \tag{11}$$

then,

$$\begin{aligned} &\rho(E0, 0^+_{\text{exc}} \to 0^+_{\text{g.s.}}) \\ &= \frac{\langle 0^+_{\text{exc}}|\hat{E}0|0^+_{\text{g.s.}}\rangle}{eR^2} = \frac{1}{eR^2}[\sqrt{\lambda(1-\lambda)}(\langle 0^+_{\text{prol}}|\hat{E}0|0^+_{\text{prol}}\rangle \\ &\quad - \langle 0^+_{\text{obl}}|\hat{E}0|0^+_{\text{obl}}\rangle) - (2\lambda - 1)\langle 0^+_{\text{prol}}|\hat{E}0|0^+_{\text{obl}}\rangle]. \end{aligned} \tag{12}$$

The cross term is neglected because the wave functions are mainly localized at different points in deformation space [13]. This expression can be written in terms of the square of the difference between the rms radii of the states which are mixed. Using an expansion of the radii in the deformation parameter β
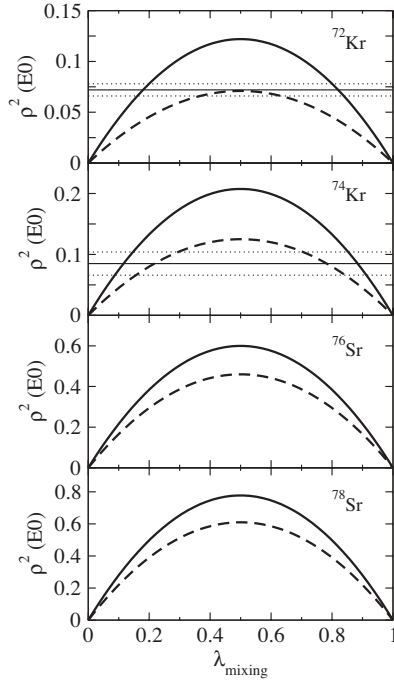
FIG. 3. Electric monopole strength $\rho^2(E0)$ with Sk3 as a function of the mixing parameter λ, calculated from Eq. (13) with (solid lines) and without (dashed lines) β^3 terms. Horizontal lines in ^{72}Kr and ^{74}Kr correspond to the experimental values from [11] and [9], respectively.

up to third order, this expression can also be written as [13,41]

$$\rho^2(E0, 0^+_{\text{exc}} \to 0^+_{\text{g.s.}})$$
$$= \lambda(1-\lambda)\left(\frac{3Z}{4\pi}\right)^2\left[\left(\beta^2_{\text{prol}} - \beta^2_{\text{obl}}\right) + \frac{5}{21}\sqrt{\frac{5}{\pi}}\left(\beta^3_{\text{prol}} - \beta^3_{\text{obl}}\right)\right]^2.$$
(13)

As one can see, if there is no mixing, the $E0$ strength becomes zero and it is largest for maximal mixing. If the deformations β are known, one can extract from these expressions the mixing of the two deformed configurations. Dynamical effects beyond mean-field approach have been considered in various works [4,42]. The results obtained from the generator coordinate method and those from the phenomenological two-level model are compared in the mass region $A = 190$. The monopole strengths calculated with both methods agree quite well [42].

Figure 3 contains the electric monopole strength $\rho^2(E0)$ obtained with the force Sk3 from Eq. (13) as a function of the mixing parameter λ. The solid (dashed) lines correspond to the results obtained with (without) the β^3 terms in Eq. (13), terms that are neglected in many works. Horizontal lines in ^{72}Kr and ^{74}Kr are the experimental values from [11] and [9], respectively. One can see that the experimental values in the Kr isotopes are compatible with $\lambda = 0.1$–0.2, which is consistent with the mixing extracted in Ref. [11] for ^{72}Kr ($\lambda_{\text{exp}} = 0.1$), but inconsistent with the mixing extracted in Ref. [12] for ^{74}Kr ($\lambda_{\text{exp}} = 0.48$). In the case of Sr isotopes, $\rho^2(E0)$ strengths are larger than in the case of Kr isotopes. Assuming that the experimental strengths are similar to those for Kr isotopes, this would indicate very weak mixing, which is
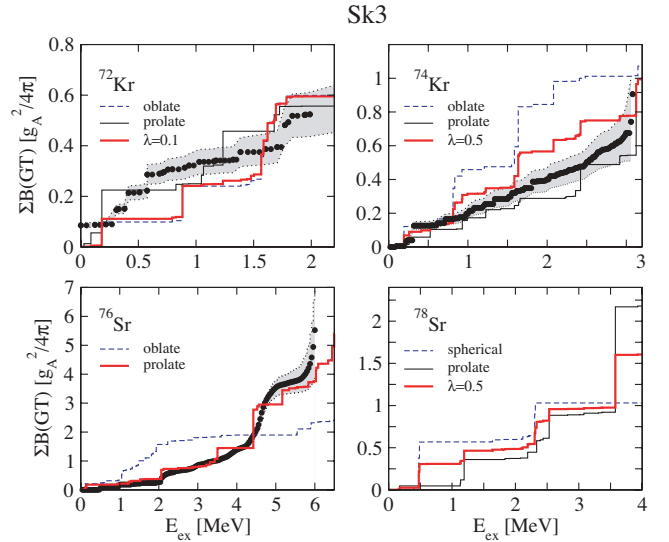

FIG. 4. (Color online) Cumulative QRPA GT strength distributions with the force Sk3 as a function of the excitation energy in the daughter nucleus. The calculations correspond to the various equilibrium configurations and to the adopted mixing. Experimental data (black dots) are from [21] (^{72}Kr), [22] (^{74}Kr), and [23] (^{76}Sr).

consistent with the strong prolate component expected in these isotopes.

B. Energy distributions of the Gamow-Teller strength

In previous works [18,26,43] we have studied the sensitivity of the GT strength distributions to the various ingredients contributing to the QRPA-like calculations, namely to the NN effective force, to pairing correlations, to deformation, and to residual interactions. We found different sensitivities to them. In this work, all of these ingredients have been fixed to the most reasonable choices found previously. Here, we mainly discuss the mixing of different shapes needed to reproduce the available experimental information on the energy distributions of GT strengths. Experimental information on GT strength distributions is available for ^{72}Kr [21], ^{74}Kr [22], and ^{76}Sr [23]. Measurements on ^{78}Sr are being presently analyzed [24]. It should be mentioned that data for ^{74}Kr, ^{76}Sr, and ^{78}Sr were taken using the total absorption gamma spectroscopy (TAgS) technique that avoids systematic uncertainties related to the so-called Pandemonium effect associated with the high resolution techniques, used for example in the case of ^{72}Kr [21]. Thus, while the GT strength has been observed over most of the Q_{EC} window in the former cases, in the latter case, only the GT strength below 2 MeV was extracted, which is still far from the $Q_{EC} = 5.04$ MeV energy.

Figures 4 and 5 show the cumulative GT strength distributions as a function of the excitation energy in the daughter nucleus. Data are compared with Sk3 and SLy4 calculations corresponding to the various equilibrium configurations and to the adopted mixing. A quenching factor 0.77 is included in these calculations. When the ground state of the parent nucleus is given by a superposition of prolate and oblate shapes
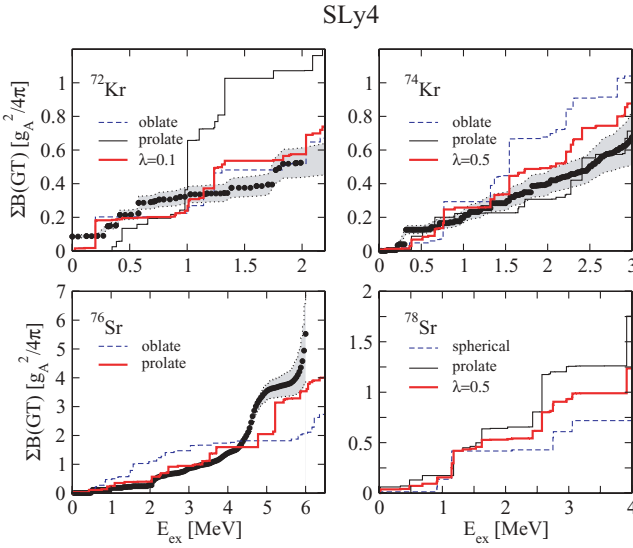
FIG. 5. (Color online) Same as in Fig. 4, but using SLy4 force.

TABLE I. Half-lives ($T_{1/2}$ [s]) corresponding to the forces Sk3 and SLy4 for the various shapes and prolate mixing λ. In the case of ^{78}Sr the oblate results correspond actually to the spherical configuration.

		oblate	prolate	mixed (λ)	exp.
Sk3					
	^{72}Kr	19.7	14.0	18.9(0.1)	17.2
	^{74}Kr	441.1	1020.0	615.9(0.5)	690
	^{76}Sr	4.2	8.9	8.9(1.0)	8.9
	^{78}Sr	93.8	320.6	145.1(0.5)	150
SLy4					
	^{72}Kr	18.2	13.7	17.6(0.1)	17.2
	^{74}Kr	718.9	858.5	782.5(0.5)	690
	^{76}Sr	5.2	10.0	10.0(1.0)	8.9
	^{78}Sr	343.4	165.9	223.7(0.5)	150

[Eq. (11)], the final 1^+ states reached by the action of the GT operator are either $|1^+_{\text{prol}}\rangle$ or $|1^+_{\text{obl}}\rangle$ at excitation energies given by ω_{prol} and ω_{obl}, respectively. Thus,

$$B_\omega(GT) = \lambda \sum_{\omega_{\text{prol}}} \langle 1^+_{\text{prol}}, \omega_{\text{prol}} | GT | 0^+_{\text{prol}} \rangle^2 \delta(\omega_{\text{prol}} - \omega)$$
$$+ (1 - \lambda) \sum_{\omega_{\text{obl}}} \langle 1^+_{\text{obl}}, \omega_{\text{obl}} | GT | 0^+_{\text{obl}} \rangle^2 \delta(\omega_{\text{obl}} - \omega). \quad (14)$$

This is certainly a simple approach that gives us only a limited insight into the more involved problem of configuration mixing, but it is a first step in this direction toward the effect of mixing in the Gamow-Teller strength distributions.

The mixing coefficients considered in these plots correspond to the experimental mixing obtained in Refs. [11,12] for the Kr isotopes. In the case of ^{76}Sr no mixing is plotted since the prolate configuration reproduces the data fairly well. In the case of ^{78}Sr, 50% mixing is plotted as a middle value useful to compare with future data. In the case of ^{72}Kr, the description of the GT strength distribution in the case of Sk3 is rather similar to both shapes. On the contrary, with SLy4, the oblate shape and in particular the mixing with a 10% prolate configuration describes the data fairly. Certainly, it would be interesting to extend the measurements up to the Q_{EC} window and compare the calculations in the whole range of energies. In the case of ^{74}Kr, the experiment is better reproduced by the prolate shape with the two Skyrme forces. However, mixing with the oblate shape improves the results although 50% mixing seems to be very strong.

The prolate configuration alone gives a good description of the GT strength distributions in ^{76}Sr with both Sk3 and SLy4 forces. The oblate shape generates a rather flat profile above 2 MeV that fails to account for the experimental profile of the strength distribution. The calculated strength distributions in ^{78}Sr show a very pronounced stepwise profile in the spherical case, as it corresponds to transitions between degenerate states.

In the prolate case the strength is more fragmented. The total accumulated strength up to about 3 MeV is similar with the two forces, but in the case of Sk3, there is a strong transition just below Q_{EC} which doubles the strength. In the case of SLy4, this strong transition occurs a little bit above $Q_{\text{EC}} = 3.76$ MeV.

These results also can be compared with other calculations such as those performed within a Tamm-Dancoff approximation with Sk3 interaction [17]. In this reference, strengths contained in bins of 1 MeV were plotted and no further details within the Q_{EC} window were shown. Nevertheless, there is qualitative agreement with our results. More recently, results from the complex excited VAMPIR variational approach with Bonn potentials, on ^{72}Kr and ^{74}Kr, have been published [19,20]. In the case of ^{72}Kr, the profile of the cumulative GT strength in Ref. [19] presents a strong jump at around 1 MeV with a continuous increase elsewhere. This is at variance with experiment which does not show this behavior. For ^{74}Kr, again a sudden increase of the strength at 1 MeV is found in [20] which does not show up in the experiment. The total strength is considerably underestimated by the calculations even though no quenching is considered in that work.

C. Half-lives

The half-lives calculated according to Eq. (9) can be seen in Table I. The results correspond to the different equilibrium deformations of the various isotopes, as well as to the mixed configurations obtained with similar mixing as those considered in Figs. 4 and 5 for the GT strength distributions. Experimental Q_{EC} values have been used in these calculations.

It should be stressed that the $f(Z, \omega)$ functions in Eq. (9) weight differently the strength depending on the energy. As a result, the half-lives are more sensitive to the strength located at certain excitation energies. One can see in Fig. 6 the $f(Z, \omega)$ functions corresponding to the β^+-decay, to the electron capture, and the total $f(Z, \omega)$ plotted versus the excitation energy of the daughter nucleus. The first thing to notice is that these factors are larger at lower excitation energies (higher
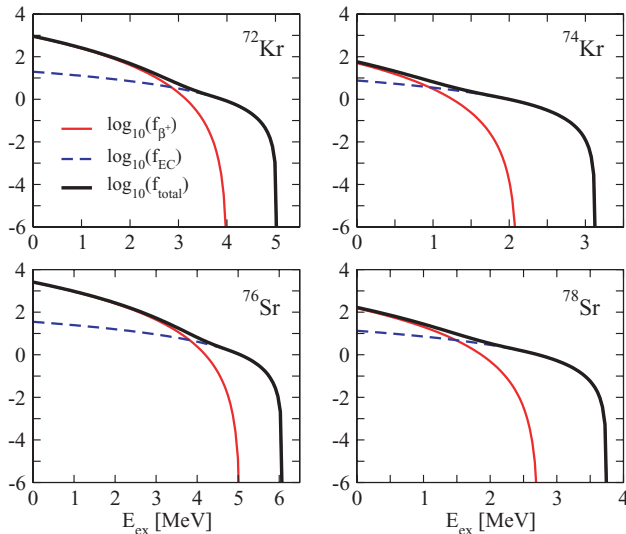
FIG. 6. (Color online) $f(Z, \omega)$ functions used in Eq. (9) to evaluate the half-lives. They are decomposed into their β^+ and electron capture (EC) components.

energy of the β-particle) and therefore, the contribution of the strength at low excitation energies to the half-lives is highly favored. One can also see that the β^+ component is the dominant contribution at lower excitation energy and it goes roughly like $(Q_\beta - E_{ex})^5$. At higher energies, electron capture becomes dominant and it is indeed the only component between Q_β and Q_{EC}, where electron capture is allowed but positron emission is energetically forbidden.

The results in Table I obtained for ^{72}Kr are once more compatible with predominantly oblate shape with a 10% prolate mixing [11], although a little bit more mixing is favored (actually the half-life is reproduced with $\lambda = 0.3$ in the case of Sk3 and with $\lambda = 0.2$ in the case of SLy4). In the case of ^{74}Kr one can see that the 50% maximal mixing considered also reproduces the experimental data reasonably well. In the case of the Sk3 force, $\lambda = 0.6$ reproduces the half-life. The half-life of ^{76}Sr is compatible with a pure prolate shape, as in the case with the GT strength distribution. In the case of ^{78}Sr, a mixing of the spherical and prolate configurations in Sk3 reproduces the half-life, while in the case of SLy4 a prolate configuration is favored.

IV. CONCLUSIONS

In this paper β-decay properties of neutron-deficient Kr and Sr isotopes are calculated within a deformed QRPA approach based on mean fields generated from self-consistent Skyrme Hartree-Fock calculations. A simple two-state mixing model has been used to mix the intrinsic configurations into the physical states. It is shown that in some cases a single shape accounts for the main characteristics of the GT strength distributions and the half-lives. In other cases the data appear between the predictions of various shapes, demanding a more sophisticated treatment. Here we have considered a rough estimate of the mixing using the same coefficients extracted phenomenologically from Coulomb excitation experiments and have found that they reproduce the GT strength distributions and half-lives fairly well. Thus, we get a globally consistent picture when describing the isotope ^{72}Kr as a mainly oblate nucleus with small admixtures from a prolate configuration, the isotope ^{74}Kr as a more mixed nucleus with a dominant prolate configuration, the isotope ^{76}Sr as an almost prolate nucleus, and the isotope ^{78}Sr as a mixed spherical/prolate nucleus.

The main objective in this paper has been to demonstrate that this approach is able to account for the main features of the decay properties of nuclei in this mass region, which are characterized by deformation as a key ingredient. This study provides additional and complementary indications in favor of shape coexistence in this mass region that is consistent with the information extracted from low-energy Coulomb excitation experiments.

This approach cannot be pushed forward at a more quantitative description since the results are not only sensitive to the details of the present calculation but may also be sensitive to dynamical effects beyond mean-field approach not considered in this work. In this respect, it is worth pointing out that multiple Coulomb excitation data are beginning to yield sufficient numbers of $E2$ matrix elements for construction not only of quadrupole centroids but also fluctuation widths for the lowest few states in even-even nuclei [44].

[1] J. L. Wood, K. Heyde, W. Nazarewicz, M. Huyse, and P. Van Duppen, Phys. Rep. **215**, 101 (1992).

[2] W. Nazarewicz, J. Dudek, R. Bengtsson, T. Bengtsson, and I. Ragnarsson, Nucl. Phys. **A435**, 397 (1985).

[3] P. Bonche, H. Flocard, P.-H. Heenen, S. J. Krieger, and M. S. Weiss, Nucl. Phys. **A443**, 39 (1985).

[4] M. Bender, P. Bonche, and P.-H. Heenen, Phys. Rev. C **74**, 024312 (2006).

[5] S. Hilaire and M. Girod, Eur. Phys. J. A **33**, 237 (2007).

[6] G. A. Lalazissis and M. M. Sharma, Nucl. Phys. **A586**, 201 (1995).

[7] A. Petrovici, K. W. Schmid, and A. Faessler, Nucl. Phys. **A605**, 290 (1996); **A665**, 333 (2000).

[8] R. B. Piercey *et al.*, Phys. Rev. Lett. **47**, 1514 (1981).

[9] C. Chandler *et al.*, Phys. Rev. C **56**, R2924 (1997).

[10] F. Becker *et al.*, Eur. Phys. J. A **4**, 103 (1999).

[11] E. Bouchez *et al.*, Phys. Rev. Lett. **90**, 082502 (2003).

[12] E. Clément *et al.*, Phys. Rev. C **75**, 054313 (2007).

[13] K. Heyde and R. A. Meyer, Phys. Rev. C **37**, 2170 (1988); **42**, 790 (1990).

[14] H. Mach, M. Moszynski, R. L. Gill, G. Molnar, F. K. Wohn, J. A. Winger, and J. C. Hill, Phys. Rev. C **41**, 350 (1990); **42**, 793 (1990).

[15] J. L. Wood, E. F. Zganjar, C. de Coster, and K. Heyde, Nucl. Phys. **A651**, 323 (1999).

[16] A. Piechaczek *et al.*, Phys. Rev. C **67**, 051305(R) (2003).

[17] F. Frisk, I. Hamamoto, and X. Z. Zhang, Phys. Rev. C **52**, 2468 (1995); I. Hamamoto and X. Z. Zhang, Z. Phys. A **353**, 145 (1995).

[18] P. Sarriguren, E. Moya de Guerra, A. Escuderos, and A. C. Carrizo, Nucl. Phys. **A635**, 55 (1998); P. Sarriguren, E. Moya de Guerra, and A. Escuderos, *ibid.* **A691**, 631 (2001).

[19] A. Petrovici, K. W. Schmid, O. Radu, and A. Faessler, Phys. Rev. C **78**, 044315 (2008).

[20] A. Petrovici, K. W. Schmid, O. Radu, and A. Faessler, Nucl. Phys. **A799**, 94 (2008).

[21] I. Piqueras *et al.*, Eur. Phys. J. A **16**, 313 (2003).

[22] E. Poirier *et al.*, Phys. Rev. C **69**, 034307 (2004).

[23] E. Nácher *et al.*, Phys. Rev. Lett. **92**, 232501 (2004).

[24] B. Rubio (private communication).

[25] H. Schatz *et al.*, Phys. Rep. **294**, 167 (1998).

[26] P. Sarriguren, R. Alvarez-Rodríguez, and E. Moya de Guerra, Eur. Phys. J. A **24**, 193 (2005).

[27] J. Krumlinde and P. Möller, Nucl. Phys. **A417**, 419 (1984); P. Möller and J. Randrup, *ibid.* **A514**, 1 (1990).

[28] H. Homma, E. Bender, M. Hirsch, K. Muto, H. V. Klapdor-Kleingrothaus, and T. Oda, Phys. Rev. C **54**, 2972 (1996).

[29] M. Hirsch, A. Staudt, K. Muto, and H. V. Klapdor-Kleingrothaus, Nucl. Phys. **A535**, 62 (1991); K. Muto, E. Bender, T. Oda, and H. V. Klapdor-Kleingrothaus, Z. Phys. A **341**, 407 (1992).

[30] M. Beiner, H. Flocard, N. Van Giai, and P. Quentin, Nucl. Phys. **A238**, 29 (1975).

[31] E. Chabanat, P. Bonche, P. Haensel, J. Meyer, and R. Schaeffer, Nucl. Phys. **A635**, 231 (1998).

[32] D. Vautherin and D. M. Brink, Phys. Rev. C **5**, 626 (1972); D. Vautherin, *ibid.* **7**, 296 (1973).

[33] G. Audi, O. Bersillon, J. Blachot, and A. H. Wapstra, Nucl. Phys. **A729**, 3 (2003).

[34] H. Flocard, P. Quentin, A. K. Kerman, and D. Vautherin, Nucl. Phys. **A203**, 433 (1973).

[35] K. Ikeda, Prog. Theor. Phys. **31**, 434 (1964); J. I. Fujita and K. Ikeda, Nucl. Phys. **67**, 145 (1965).

[36] A. Bohr and B. Mottelson, *Nuclear Structure* (Benjamin, New York, 1975), Vol. II, p. 10.

[37] G. F. Bertsch and I. Hamamoto, Phys. Rev. C **26**, 1323 (1982).

[38] N. B. Gove and M. J. Martin, Nucl. Data Tables **10**, 205 (1971).

[39] P. Möller, J. R. Nix, W. D. Myers, and W. J. Swiatecki, At. Data Nucl. Data Tables **59**, 185 (1995).

[40] C. J. Lister, P. J. Ennis, A. A. Chishti, B. J. Varley, W. Gelletly, H. G. Price, and A. N. James, Phys. Rev. C **42**, R1191 (1990).

[41] J. O. Rasmussen, Nucl. Phys. **19**, 85 (1960); A. S. Davydov, V. S. Rostovsky, and A. A. Chaban, *ibid.* **27**, 134 (1961); J. P. Davidson, Rev. Mod. Phys. **37**, 105 (1965).

[42] H. Dancer, P. Bonche, H. Flocard, P.-H. Heenen, J. Meyer, and M. Meyer, Phys. Rev. C **58**, 2068 (1998).

[43] P. Sarriguren, E. Moya de Guerra, and A. Escuderos, Nucl. Phys. **A658**, 13 (1999); Phys. Rev. C **64**, 064306 (2001); P. Sarriguren, O. Moreno, R. Alvarez-Rodriguez, and E. Moya deGuerra, *ibid.* **72**, 054317 (2005).

[44] D. Cline, Annu. Rev. Nucl. Part. Sci. **36**, 683 (1986).